



HAL
open science

Substituent-Induced Control of *fac* / *mer* Isomerism in Azine-NHC Fe(II) Complexes

Ulises Carrillo, Antonio Francés-Monerris, Anil Reddy Marri, Cristina Cebrián, Philippe Gros

► **To cite this version:**

Ulises Carrillo, Antonio Francés-Monerris, Anil Reddy Marri, Cristina Cebrián, Philippe Gros. Substituent-Induced Control of *fac* / *mer* Isomerism in Azine-NHC Fe(II) Complexes. ACS Organic & Inorganic Au, 2022, 10.1021/acscorginorgau.2c00038 . hal-03793259

HAL Id: hal-03793259

<https://hal.science/hal-03793259v1>

Submitted on 15 Nov 2022

HAL is a multi-disciplinary open access archive for the deposit and dissemination of scientific research documents, whether they are published or not. The documents may come from teaching and research institutions in France or abroad, or from public or private research centers.

L'archive ouverte pluridisciplinaire **HAL**, est destinée au dépôt et à la diffusion de documents scientifiques de niveau recherche, publiés ou non, émanant des établissements d'enseignement et de recherche français ou étrangers, des laboratoires publics ou privés.

Substituent-Induced Control of *fac/mer* Isomerism in Azine-NHC Fe(II) Complexes

Ulises Carrillo, Antonio Francés-Monerris, Anil Reddy Marri, Cristina Cebrián,* and Philippe C. Gros*

Cite This: <https://doi.org/10.1021/acsorginorgau.2c00038>

Read Online

ACCESS |



Metrics & More



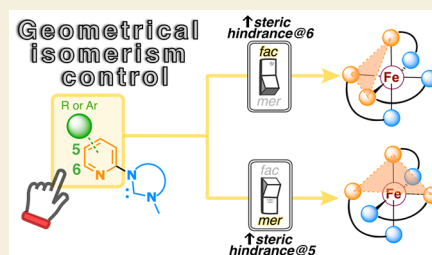
Article Recommendations



Supporting Information

ABSTRACT: The stereoselective synthesis of geometrical iron(II) complexes bearing azine-NHC ligands is described. Facial and meridional selectivity is achieved as a function of the steric demand of the azine unit, with no remarkable influence of the carbene nature. More specifically, meridional complexes are obtained upon selecting bulky 5-mesityl-substituted pyridyl coordinating units. Unexpectedly, increase of the steric hindrance in the α position with respect to the N coordinating atom results in an exclusive facial configuration, which is in stark contrast to the meridional selectivity induced by other reported α -substituted bidentate ligands. Investigation of the structure and the optical and electrochemical properties of the here-described complexes has revealed the non-negligible effect of the *fac/mer* ligand configuration around the metal center.

KEYWORDS: Bidentate ligands, computational calculations, *fac/mer* isomers, iron complexes, NHC ligands



INTRODUCTION

The stereoselective synthesis of octahedral complexes with unsymmetrical bidentate ligands $M(A^*B)_3$ keeps attracting considerable interest due to the intrinsic relationship between molecular structure and resulting properties. Indeed, it is well-known that coordination of this type of ligands often results in a mixture of facial and meridional stereoisomers in a statistical 1:3 ratio (Figure 1a).¹ However, these isomers can have different photophysical, electrochemical, and magnetic properties,^{2–5} with appealing applications in OLEDs,^{2,6,7} catalysis^{7,8} or supramolecular chemistry.^{9–11} Considering that isolation of these isomers can be extremely challenging, especially in the case of labile complexes, attaining control over the *fac/mer* stereoisomerism is thus of great importance.

In the most general case, the synthesis of facial isomers is enthalpically-driven, which is at the origin of the so-called trans effect,¹² while that of the meridional congeners is entropically-driven.¹³ Nevertheless, systematic deviations from these statements are commonly encountered due to steric reasons or the presence of additional intra-/intermolecular interactions.¹ Interestingly, strategies based on solvation effects,^{10,14} supramolecular interactions,^{15–18} the use of preorganized platforms,^{11,19–23} and exposure to external stimuli such as heat^{24–26} or light^{24,27} have been shown to influence the *fac/mer* ratio.

On the other hand, the development of photoactive iron complexes is currently a hot topic within the scientific community. Despite the challenging photophysics of typical polyimine Fe complexes, charge transfer-excited states with lifetimes ranging from hundred of picoseconds^{28,29} up to few nanoseconds^{3–32} have been achieved. These impressive results

are the consequence of judicious ligand designs, with N-heterocyclic carbenes (NHC),^{29,30} cyclometalating³¹ units, or amides³² playing a pivotal role in the creation of sufficiently high ligand fields.

During our recent research works in this field, we have reported a series of bidentate pyridyl-NHC iron (II) complexes with lifetimes comparable to those of their tridentate analogues while having one NHC unit less.⁵ Although the metal–ligand interaction was improved, the asymmetry of the ligands led to the obtention of geometrical isomers (Figure 1b). In the case of C0 comprising pyridine-imidazol-2-ylidene ligands, a 1:14 *fac/mer* ratio was obtained.³³ In stark contrast to typical Fe^{II} complexes, no lability was observed for C0. However, isolation of these geometric isomers was not attained. As a result, molecular modeling was selected to provide some insights into the photophysical properties of these distinct species, especially regarding their excited state properties. Interestingly, these results showed that, upon electronic excitation, the facial configuration leads to slower relaxation kinetics, resulting in longer excited state lifetimes.^{33,34} Subsequent preparation of a pure facial complex was possible by means of the tripodal C₃ ligand L1.²³ Nevertheless, the influence of the connecting scaffold and the increased rigidity on the final properties of the facial isomer cannot be ruled out. Increase of the π -conjugation

Received: July 13, 2022

Revised: September 12, 2022

Accepted: September 13, 2022

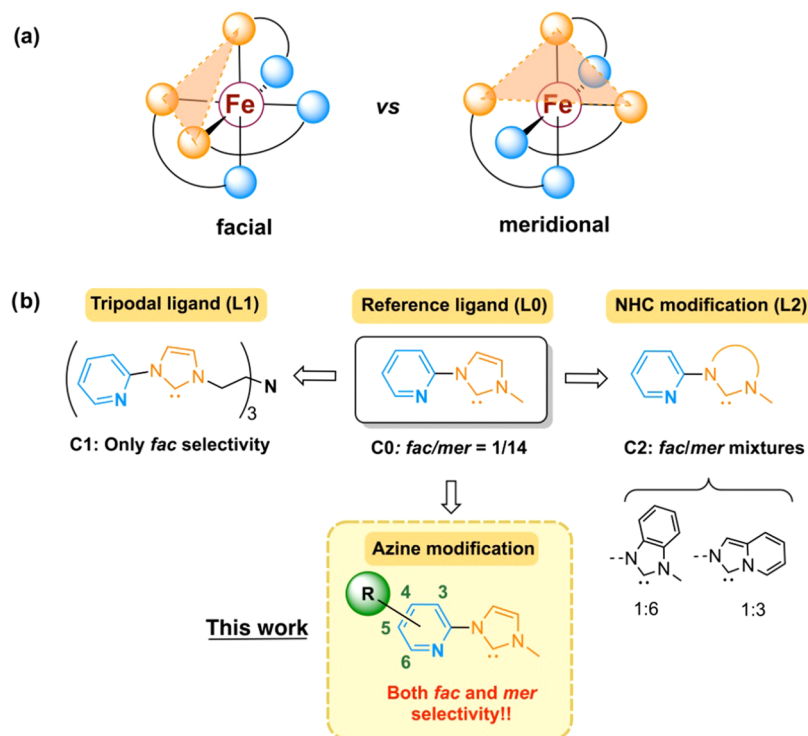
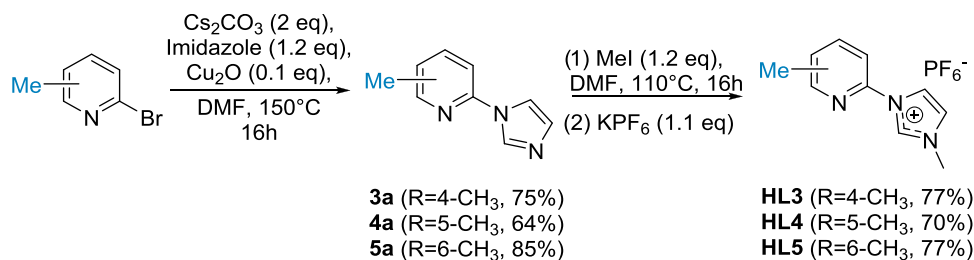
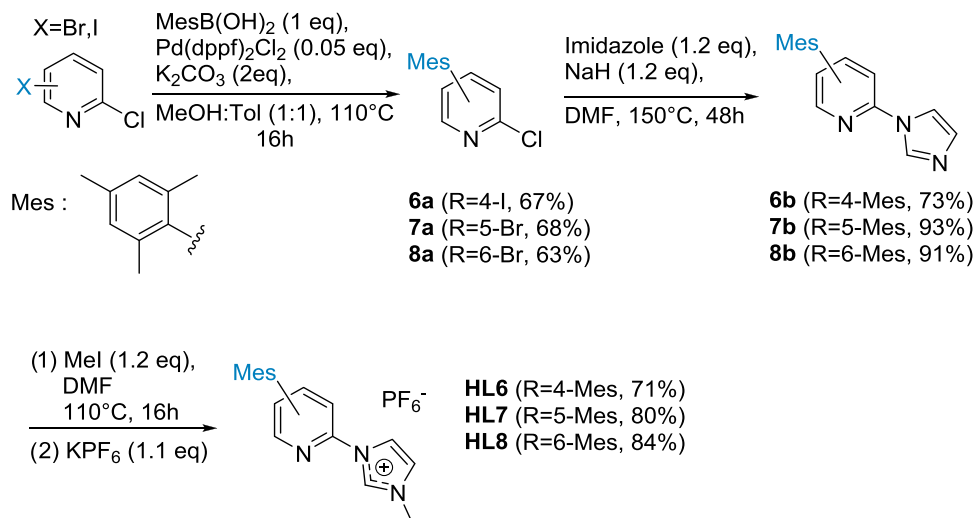


Figure 1. (a) Schematic representation of facial and meridional configurations for iron(II) complexes bearing asymmetric bidentate ligands. (b) Overview of the explored ligand designs and their impact on the *fac/mer* ratio of the corresponding iron(II) complexes.

Scheme 1. Synthesis of Ligand Precursors HL3–HL5



Scheme 2. Synthesis of Ligand Precursors HL6–HL8



at the NHC unit (L2 ligands) afforded opposite modulations of the opto-electronic properties depending on the localization of the benzannulated ring.³⁵ Noteworthy, the increased steric

demand of the ligands leads to a modification of the stereoselectivity toward higher *fac/mer* ratios with respect to parent L0, highlighting the importance of a rational ligand

design. Prompted by these results and the need to exert precise control on the coordination sphere, we explore in this contribution the effects of modifying both the substitution nature and pattern at the azine unit on the final complex configuration, which turns out to be pivotal for *fac/mer* isomer selectivity (Figure 1b). In particular, an unexpected facial selectivity is provided by 6-substituted pyridyl-/quinolyl-/quinoxalyl-NHC ligands which is, to the best of our knowledge, unique for this type of sterically demanding bidentate ligands.

RESULTS AND DISCUSSION

Two different ligand precursor series were initially prepared for the introduction of two levels of steric hindrance. A methyl (Me) (HL3–HL5) was selected as the low level to minimize the inductive or resonance effects (Scheme 1). A mesityl (Mes) group (HL6–HL8) was chosen instead as the high level not only due to its high steric demand but also because of the additional possibility of promoting π -stacking interactions (Scheme 2).³⁶ Substitution was performed at positions 4, 5, and 6 at the pyridine moiety for both series. Position 3 was not functionalized since a weaker interaction with the metal ion could be anticipated due to the concomitant loss of coplanarity upon such ligand modification.⁴

In all cases, pyridyl-imidazoliums were selected for the preparation of py-NHC bidentate ligands. Me-based precursors HL3–HL5 were obtained in good yields by an Ullmann coupling of imidazole on the corresponding methylated 2-bromopyridine, followed by a quaternization with iodomethane in DMF at 110 °C and final metathesis with potassium hexafluorophosphate (Scheme 1). As for Mes-based precursors HL6–HL8, their synthesis was conceived from halogenated 2-chloropyridines. After the initial selective introduction of the mesityl group by means of a Suzuki coupling, the imidazole unit was introduced via a S_N^Ar mechanism at the Cl-substituted pyridine position. Upon azole quaternization with MeI and I^- to PF_6^- counterion metathesis, the target precursors were obtained in good yields (Scheme 2).

Based on our previous works with unsubstituted ligands, the complexation of HL3–HL8 precursors was performed using $FeCl_2$ as iron source, KHMDS as the base, and DMF as solvent (Table 1). With the exception of L8, successful ligand coordination yielded C3–C7 in ca. 45%, regardless of the

ligand nature. Nevertheless, remarkable differences were obtained concerning the *fac/mer* selectivity. Within the Me-based series, no significant influence was observed for L3 and L4, with the methyl group at 4 and 5 positions, respectively, obtaining C3 and C4 with a near statistic 1:3 *fac/mer* ratio (entries 1 and 2). However, the presence of the methyl group adjacent to the pyridinic N atom in L5 nicely resulted in the exclusive formation of the facial isomer *fac*-C5 despite its non-negligible steric hindrance toward the metal ion coordination (entry 3). This result was completely unexpected since previously reported 6-methyl-2,2'-bipyridine complexes resulted in meridional complexes.³⁷ Moreover, the complex remains in its low-spin configuration, which also differs from other similarly substituted facial complexes.^{38,39}

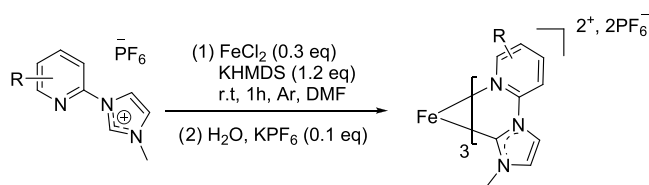
Concerning the bulkier Mes group, no influence on the final configuration was again observed when substituted at position 4 (ligand L6) due to its outward directionality, obtaining the corresponding facial and meridional C6 complexes as a statistical 1 to 3 mixture (entry 4). Nevertheless, the presence of the Mes group at position 5 leads to very crowded environments, notably in a facial configuration. As a result, ligand coordination yielded almost exclusively *mer*-C7 complex (entry 5). Unfortunately, coordination of ligand L8 with the Mes group adjacent to the pyridinic N atom was unsuccessful, even upon increasing the reaction temperature or performing the carbene before adding the iron source (entry 6). It is worth noting that similar substitutions at the 5-membered NHC moiety in related Fe^{II} Py-NHC complexes have been described.³⁶ However, the smaller angle formed between the Mes group and the Fe–N bond due to the 6-membered pyridine ring is likely to increase the steric hindrance to such an extent that coordination is completely inhibited.

To evaluate the excellent selectivity toward *fac* and *mer* geometries promoted by L5 (6-Me) and L7 (5-Mes), we subsequently examined the impact of the NHC electronic nature. Thus, besides imidazole-based (Im) precursors, two additional ones were prepared for each substitution pattern from benzimidazole (BIm) and 4-methylimidazole (4-MeIm), which would afford more π -acceptor and more σ -donor NHC units, respectively. The synthesis of the NHC-varying ligand precursors HL9–HL12 is depicted in Scheme 3.

Using the previously described complexation conditions (see Table 1), target C9–C13 complexes were obtained in moderate yields (40–49%) (Table 2). As it can be observed, electronic properties of the NHC unit did not affect either the facial coordination selectivity with a 6-Me substitution (entries 1–3) or the meridional selectivity in the case of the 5-Mes substitution (entries 4–6), attaining even a complete selectivity for both configurations with the facial or meridional congeners remaining at best below the detection limit in 1H NMR. Therefore, these results nicely indicated that the final configuration of the system is mostly determined by the azine substitution pattern in py-NHC complexes.

The remarkable and unanticipated facial selectivity exerted by the 6-Me substituted ligands L5, L9, and L10 spurred us on to investigate the exact role played by this group. As a result, a new series of ligand precursors was prepared with varying functionalities at this position, including a more sterically hindered isopropyl (iPr) chain (HL13), several halogenated substituents (HL14–HL16), and a dimethylamine (NMe_2) group (HL17) (Figure 2). As shown in Scheme S3 (see the Supporting Information (SI)), HL13–HL17 were prepared following rather similar synthetic protocols, as previously

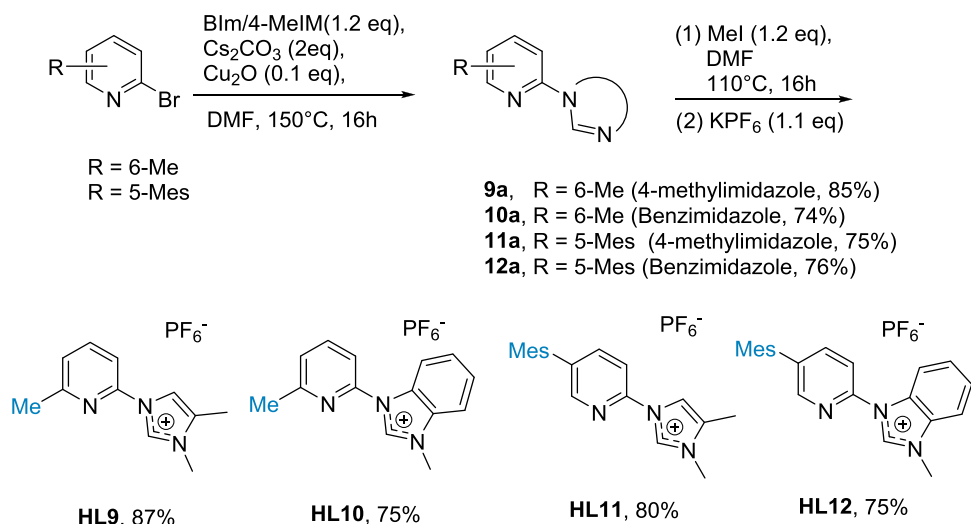
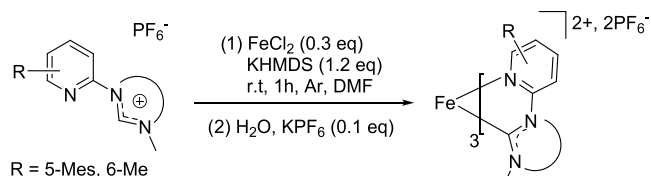
Table 1. Effect of the Ligand Steric Demand on Fe^{II} Complex Formation



entry	ligand precursor	yield (%) ^a	<i>fac/mer</i> ratio ^b	complex
1	HL3 (4-Me)	44	25:75	C3
2	HL4 (5-Me)	44	20:80	C4
3	HL5 (6-Me)	45	98:2	<i>fac</i> -C5
4	HL6 (4-Mes)	48	25:75	C6
5	HL7 (5-Mes)	45	4:96	<i>mer</i> -C7
6	HL8 (6-Mes)			

^aIsolated yield. ^b*fac/mer* ratio determined by 1H NMR.

Scheme 3. Synthesis of Ligands HL9–HL12

Table 2. Effect of the Nature of the NHC Unit on the Fe^{II} Complex Formation. Data from HL5 and HL7 are Presented for Comparison Reasons

entry	ligand precursor	yield (%) ^a	fac/mer ratio ^b	complex
1	HL5 (6-Me, Im)	45	98:2	fac-C5
2	HL9 (6-Me, 4-MeIm)	48	100:0	fac-C9
3	HL10 (6-Me, blm)	43	100:0	fac-C10
4	HL7 (5-Mes, Im)	45	4:96	mer-C7
5	HL11 (5-Mes, 4-MeIm)	49	0:100	mer-C11
6	HL12 (5-Mes, blm)	40	0:100	mer-C12

^aIsolated yield. ^bfac/mer ratio determined by ¹H NMR.

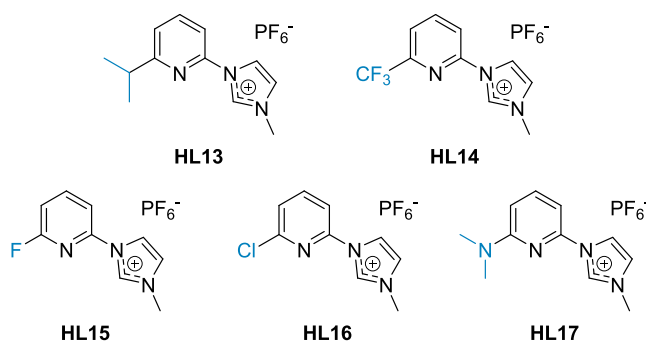
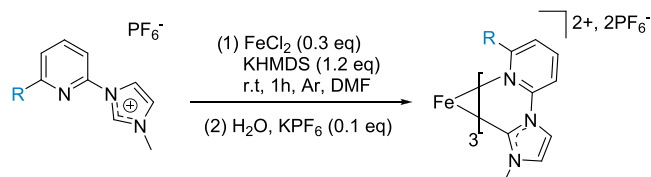


Figure 2. Series of ligand precursors with varying 6-substituted pyridine moieties.

described, starting from the appropriately substituted 2-halopyridine. In the case of HL13 and HL17, previous introduction of their respective ⁱPr and NMe₂ groups was necessary.

The complexation results of precursors HL13–HL17 are gathered in Table 3. The introduction of an ⁱPr group provided the same effect as a methyl group, *i.e.*, an exclusive facial isomerism, affording fac-C13 in 30% yield (entry 1). The

Table 3. Coordination with Different Substituents at Position 6 on the Pyridine Moiety



entry	ligand precursor	yield (%) ^a	fac/mer ratio ^b	complex
1	HL13 (R = ⁱ Pr)	40	100:0	fac-C13
2	HL14 (R = CF ₃)			
3	HL15 (R = F)			
4	HL16 (R = Cl)	18	100:0	fac-C16
5	HL17 (R = NMe ₂)			

^aIsolated yield. ^bfac/mer ratio determined by ¹H NMR, with ≥1% as the detection limit.

electron-withdrawing halogenated substituents had more differing results (entries 2–4). Indeed, while no complex was obtained with L14 (6-CF₃) and L15 (6-F) attributable to an excessively reduced basicity of the pyridine, L16 (6-Cl) led exclusively to fac-C16 complex though in rather a poor yield (18%). This latter example is, however, of particular interest since it would allow for complex functionalization via cross-couplings or S_N^{Ar} reactions, for instance. In the case of the electron-donating NMe₂ group, no complex was isolated (entry 5). A tentative explanation for this could be a competitive coordination of the amino group to the metal ion that would probably inhibit the coordination of the NHC moiety. In consequence, from these results, we can infer that facial selectivity is not necessarily led by an agnostic interaction between the hydrogens of the methyl group and the pyridine ring since selectivity was not compromised with –Cl and –ⁱPr substituents.

Given that the 6-CH₃ substituent could provide a similar steric hindrance as an internal –CH– of a phenyl group (Figure 3), we decided to examine the effect of extending the π-conjugation at the azine moiety as well.

Ligand precursors derived from quinoline (HL18) and quinoxaline (HL19) were thus synthesized (Scheme 4). HL18 was prepared in 75% yield in a 2-step synthesis by reacting 2-

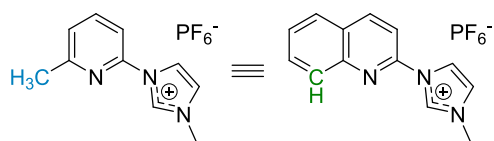


Figure 3. Steric Hindrance of CH₃ Compared to Internal CH.

chloroquinoline with *in situ*-generated potassium imidazolate, followed by quaternization with MeI. The higher reactivity of 2-chloroquinoxaline toward a S_N^{Ar} reaction allowed HL19 to be directly obtained in 77% yield upon reaction with *N*-methylimidazole. The complexation of both π -extended HL18 and HL19 precursors was carried out under the same aforementioned conditions using FeCl₂ and KHMDS in DMF at r.t. (Scheme 4). Gratifyingly, the results were consistent with our hypothesis since the coordination afforded exclusively *fac*-C18 and *fac*-C19 complexes in 37 and 34% yield, respectively. As in the case of 6-Me (*fac*-C5) pyridine-based ligands, these results are in stark contrast with the stereochemistry obtained with other related ligands such as 2-(pyridin-2-yl)quinoline, which lead to the exclusive formation of the meridional isomer.⁴⁰

X-RAY ANALYSIS

Suitable crystals of *fac*-C5, *mer*-C7, and *fac*-C18 for X-ray diffraction were grown by slow evaporation of the corresponding methanol (*fac*-C5) or acetonitrile (*mer*-C7 and *fac*-C18) solutions (see Table S1 and Figures SS90–S92). Figure 4 gathers the structures for the three complexes, displaying a distorted octahedral geometry and confirming the anticipated configurations. Some selected structural parameters are collected in Table 4.

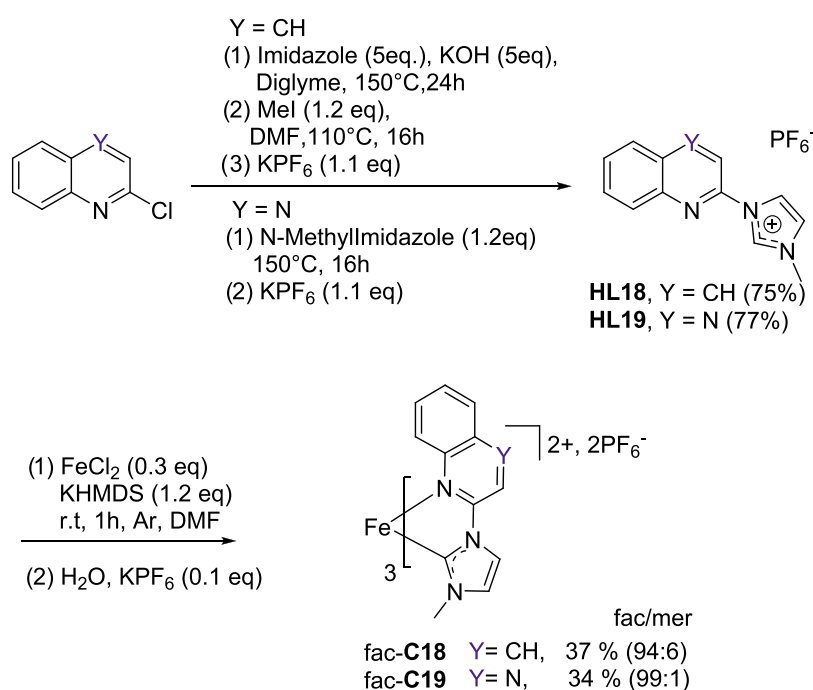
Both structures of *fac*-C5 and *fac*-C18 show three bidentate ligands with the same orientation, resulting in a facial arrangement with each Fe–C bond trans to a Fe–N bond. In comparison to the computationally optimized structure of

fac-C0,³³ average Fe–C bond distances (1.904 Å for *fac*-C5 and 1.899 Å for *fac*-C19 vs 1.948 Å for *fac*-C0) are significantly shorter, while average Fe–N bond distances are only slightly shorter (2.141 Å for *fac*-C5 and 2.138 Å for *fac*-C18 vs 2.072 Å for *fac*-C0). Nevertheless, the steric hindrance exerted by the imine unit is more evident when analyzing the conformation of the bidentate units, which exhibit marked tilting angles of 4.4–13.1 and 5.1–10.4° for *fac*-C5 for *fac*-C18, respectively. Thus, it would be tempting to correlate the enhanced structural trans effect in *fac*-C5 and *fac*-C18 with respect to *fac*-C0 with a higher kinetic trans effect, which would explain the obtained selectivity, but knowledge of the complexation mechanism is required.¹²

Furthermore, it is worth noting the presence of several short contacts in these facial complexes. These interactions involve mostly the coordinated atoms (C_{carbene} or N_{azine}) to the iron center with a neighboring CH₃ group ($d + 0.2 \text{ \AA} < \text{sum of the van der Waals radii}$) for both *fac*-C5 and *fac*-C18, or N_{quinoline}...H–C_{quinoline}⁸ ($d + 0.4 \text{ \AA} < \text{sum of the van der Waals radii}$) in the case of *fac*-C18. Since C_{carbene}...Cl intramolecular interactions have been reported,⁴² this type of short contacts might be also envisaged for *fac*-C16. As a result, it could be likely that these interactions play a non-negligible role in the here-obtained facial selectivity.

The structure of complex *mer*-C7 shows, on the contrary, a meridional arrangement where only two ligands are oriented in the same direction, resulting in a C₁ symmetry. While the mutually trans Fe–C and Fe–N bonds are rather comparable to those in the facial complexes, more remarkable differences are observed for the other four metal–ligand bonds. In fact, the mutually trans Fe–C bonds are longer (~1.945 Å) and the mutually trans Fe–N bonds are shorter (~1.981 Å) than those in *fac*-C5 and *fac*-C18, being consistent with the stronger trans effect of a carbene ligand relative to an azine moiety. Moreover, the less crowded coordination sphere allows the ligands to adopt almost coplanar conformations (tilting angles = 0.20–

Scheme 4. Synthesis of Ligand Precursors HL18 and HL19 and Synthesis of Complexes *fac*-C18 and *fac*-C19



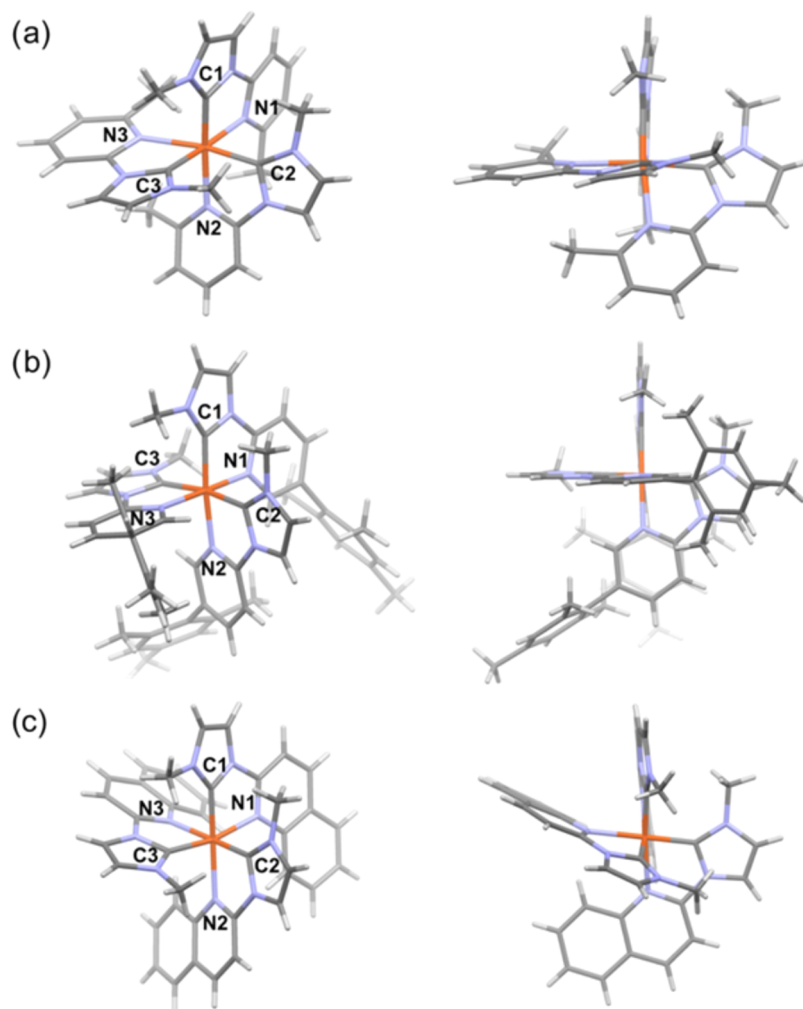


Figure 4. Left View from the (pseudo)- C_3 axis and (right) side view of the X-ray crystal structures of complexes (a) *fac*-C5, (b) *mer*-C7, and (c) *fac*-C18 with a partial labeling. Periphery atoms on the ligands are omitted for more clarity. CCDC for *fac*-C5: 2126499; *mer*-C7: 2126506; and *fac*-C18: 2126500.

Table 4. Selected Structural and Deformation Parameters for Complexes *fac*-C5, *fac*-C18, and *mer*-C7 (esd in Parenthesis)^a

	<i>fac</i> -C0	<i>fac</i> -C5	<i>fac</i> -C18	<i>mer</i> -C0	<i>mer</i> -C7
Fe-N1 (Å)	2.073	2.105(3)	2.137(2)	2.038	1.975(3)
Fe-N2 (Å)	2.072	2.131(2)	2.135(2)	2.082	2.015(2)
Fe-N3 (Å)	2.070	2.188(2)	2.142(2)	2.042	1.988(3)
Fe-C1 (Å)	1.949	1.893(3)	1.907(2)	1.942	1.903(3)
Fe-C2 (Å)	1.950	1.910(3)	1.899(2)	1.992	1.934(3)
Fe-C3 (Å)	1.947	1.910(3)	1.892(2)	1.983	1.956(3)
C1-Fe-N2 (°)	172.6	174.1(1)	168.6(9)	173.2	173.4(1)
C2-Fe-N3 (°)	172.8	169.9(1)	173.6(9)		
C3-Fe-N1 (°)	172.7	176.6(1)	176.1(9)		
C2-Fe-C3 (°)				170.0	169.9(1)
N1-Fe-N3 (°)				177.0	177.8(1)
$\langle Fe - X \rangle$ (Å) ^b	2.010	2.023	2.019	2.013	1.962
ζ (Å) ^c	0.368	0.710	0.717	0.245	0.185
Σ (°) ^d	64.9	81.4	85.9	67.7	61.2
Θ (°) ^e	205.1	241.2	257.0	213.3	196.4

^aThe Deformation Parameters were Calculated with OctaDist.⁴¹ For the Sake of Comparison, Data for DFT-Optimized *fac*-C0 and *mer*-C0 are Provided as Well, with Partial Labeling Analogous *fac*-C5 and *mer*-C7, Respectively.²³ ^bAverage metal–ligand bond. ^cLength distortion calculated as $\xi = \sum_{i=1}^6 (d_i - \langle Fe - X \rangle)$, with d_i being a metal–ligand bond. ^dAngle distortion calculated as $\Sigma \sum_{i=1}^{12} |90 - \phi_i|$ with ϕ_i being a *cis* ligand–metal–ligand angle. ^eTrigonal distortion calculated as $\Theta = \sum_{i=1}^{24} |60 - \theta_i|$, with θ_i being a torsional angle between the ligand atoms on opposite triangular faces of the octahedron viewed along the pseudo-threefold axis.

2.38°), resulting in fewer intramolecular short contacts mainly consisting of $L \cdots H-C_{\text{pyridine}}^6$ ($L = C_{\text{carbene}}$ or N_{azine}).

A more global comparison can be further done upon calculation of the stretching (ζ), angular (Σ), and trigonal (Θ) distortions from the ideal octahedral structure (Table 4).⁴¹ Taking as reference the calculated structures of *fac*-C0, it is evident that the deformation was induced by the sterically demanding azine unit, with an increased asymmetry in bond lengths (ζ values) and worse M–L interaction (Σ and Θ values, with $\Sigma = 0^\circ$ and $\Theta = 0^\circ$ for a perfect octahedron). Interestingly, complex *mer*-C7 displays the most regular coordination sphere even when compared with parent *mer*-C0.

THEORETICAL CALCULATIONS

The structural and energetic differences between the *fac* and *mer* isomers for some of the complexes synthesized in this work have been studied with quantum chemistry methodologies to better understand the observed isomer preferences. Geometry optimizations were performed with the density functional theory (DFT) method in acetonitrile.^{43–46} Final energies, computed on top of the optimized geometries, were determined with the post-Hartree–Fock method domain-based local pair natural orbital coupled-cluster singles, doubles, and perturbative triples [DLPNO-CCSD(T)].^{47,48} The latter method provides energies close to the full CCSD(T) procedure,⁴⁹ the gold standard in quantum chemistry, prohibitive for large-size molecules like the ones synthesized in this work. Solvent effects for ACN or DMF provide almost indistinguishable results (Table S2). Full computational details are included in the SI.

The *fac* vs *mer* thermodynamic stabilities are shown in Figure 5. It becomes apparent that the *fac* disposition is the

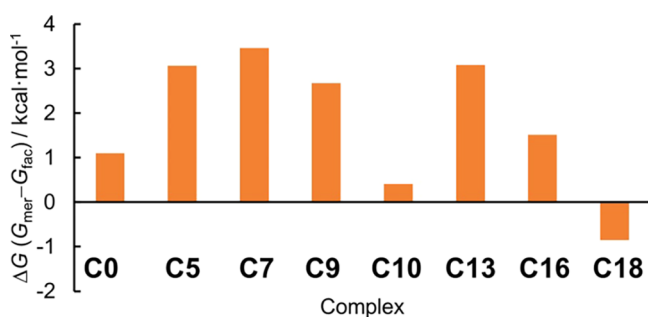


Figure 5. Gibbs energy difference (ΔG) between the *fac* and *mer* isomers for some selected complexes synthesized in this work. Optimized geometries and vibrational frequencies computed at the DFT/B3LYP-D3 level of theory. Energies refined with the DLPNO-CCSD(T) method in DMF.

most stable configuration for most of the Fe^{II} -NHC family, a trend that globally agrees with the *fac* preference observed experimentally. However, more specific analyses reveal that the thermodynamic stabilities of the isomers are not the only factors dictating the *fac/mer* preferences, suggesting that other factors also play an important role. These factors would include complexation kinetics and/or intramolecular interactions, as previously suggested.

The Gibbs energy differences between the two isomers are not equal for all complexes (Figure 5). Whereas C5, C7, C9, and C13 clearly favor the *fac* disposition ($\Delta G \sim 3$ kcal/mol), complexes C0, C10, and C18 show almost degenerated energies for both *fac* and *mer* arrangements ($\Delta G \sim \pm 1$ kcal/

mol). This is coherent with the *fac/mer* isomer distribution (6.6:93.4) observed for C0²³ and the *fac* preference (>98:2) exhibited by C5, C9, and C13. An eye-chasing case is C7, synthesized mostly as a *mer* isomer, although the *fac* disposition is thermodynamically more stable. This evidences that the complexation mechanism penalizes the *fac* isomer. Meanwhile, the ΔG values for C10 and C18 also do not explain the *fac/mer* ratio higher than 94:6 as observed experimentally in terms of thermodynamic stabilities, again pointing to extrinsic factors in the complexation process.

A particularly interesting comparison is that of complexes C0 and C5. Both compounds only differ in the methyl group at the 6 position of the pyridine ring in C5, which is key to inducing opposite isomer preferences: C0 is mostly *mer*, whereas C5 is *fac*. A detailed analysis of the Fe–N and Fe–C connections, as well as the noncovalent interactions between the methyl groups and the C and N dative atoms coordinated to iron, is presented in Figure 6 and Table 5. For *fac*-C5, the

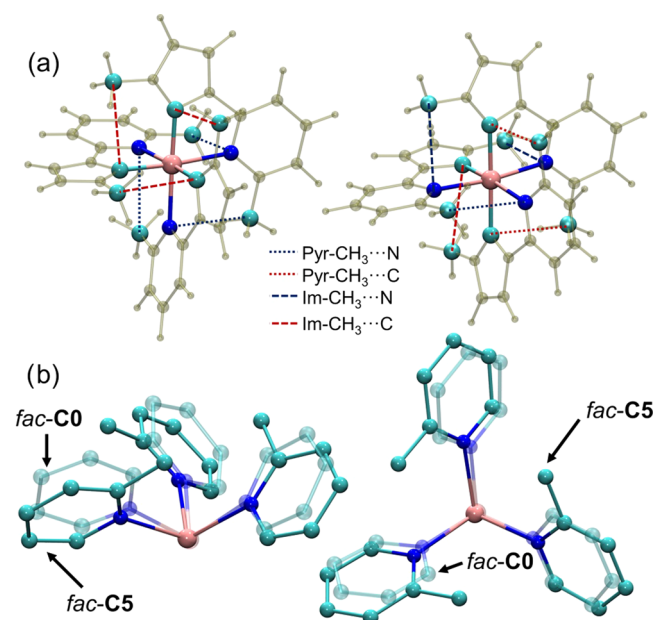


Figure 6. (a) DFT/B3LYP-D3-optimized structures of the *fac* (left) and *mer* (right) isomers for C5 and nomenclature of the intramolecular noncovalent interactions. (b) Side (left) and top (right) views of the *fac* isomer of C0 (transparent texture) and C5 (solid texture). For the sake of clarity, only the Fe centers and the pyridine rings are shown.

distances clearly indicate that the methylation at the 6 position of the pyridine enlarges the three Fe–N distances 0.134 Å (on average) due to steric congestion of the three methyl groups. This effect is illustrated in Figure 6b. As a result, on the opposite side of the molecule, the Fe–C and the Im-CH₃⋯C distances decrease by −0.005 and −0.051 Å, respectively (Table 5). Regarding *mer*-C5, the structural deformation is similar. On average, the Fe–N distances increase by 0.114 Å, and the Fe–C distances decrease by −0.004 Å, respectively. The largest difference between the *mer* isomers of C0 and C5 is found for the Im-CH₃⋯C and Im-CH₃⋯N distances, which decrease by −0.072 Å.

Globally, the net structural deformations upon methylation from C0 to C5 are almost equal for both isomers, even though the deformation is not equally distributed into the same

Table 5. Relevant Interatomic Distances (in Å) for the Optimized Structures of *fac* and *mer* Isomers of C0 and C5 as Defined in Figure 6

bond/interaction	<i>fac</i> -C0	<i>fac</i> -C5	<i>mer</i> -C0	<i>mer</i> -C5
Fe–N	2.057	2.195	2.065	2.126
	2.057	2.190	2.030	2.200
	2.057	2.189	2.025	2.135
Fe–C	1.931	1.926	1.927	1.977
	1.930	1.926	1.968	1.917
	1.931	1.926	1.974	1.963
Im-CH ₃ ⋯C	3.175	3.117	3.205	3.166
	3.174	3.135		
	3.172	3.117		
Im-CH ₃ ⋯N			3.224	3.136
			3.209	3.121
Pyr-CH ₃ ⋯C				3.047
				3.005
Pyr-CH ₃ ⋯N		3.045		3.023
		3.043		
		3.039		

molecular parameters. These subtle—yet important—differences impact the relative stability of both isomers. As a matter of fact, the thermodynamic stability of *fac*-C5 is about ~2 kcal/mol larger than that of *fac*-C0 with respect to the respective *mer* counterparts (Figure 5). This difference is the combination of diverse attractive and repulsive interactions. In this regard, the more pronounced stretching of the more labile Fe–N bonds (as compared to Fe–C) in *fac*-C5, as well as the more favorable Pyr-CH₃⋯N noncovalent interactions (as compared to the Pyr-CH₃⋯C), in which the methyl group can act as a Lewis base⁵⁰ and the N as a Lewis acid (N is more electronegative than C and thus more acidic), may explain the slight energetic differences.

The noncovalent interactions available only in *fac* arrangements also explain the stability of the *fac*-C7 structure with respect to the *mer* isomer. The *fac* arrangement clearly shows triple T-stacking interactions between the methyl groups of the mesityl substituent and the aromatic rings (Figure 7), whereas,

in the *mer* disposition, only two 5-Mes groups interact due to intrinsic reasons. It can be hypothesized that the reason to obtain C7 mainly as a *mer* isomer (Table 2) is likely due to steric congestion in the complexation mechanism. This analysis evidences again the need to consider mechanistic and other extrinsic factors besides the intrinsic stability of the isomers to fully understand the *fac/mer* isomerism in this kind of Fe^{II}-NHC complexes.

GROUND-STATE CHARACTERIZATION

Optical and electrochemical properties of all facial and meridional complexes were investigated by UV–vis spectroscopy (Figure 8) and cyclic voltammetry (see Figures S93–S102), and the main results are collected in Table 6. As in previously reported compounds,⁵ the UV–vis spectra of all complexes present three main absorption bands. The intense bands below 300 nm correspond to $^1(\pi \rightarrow \pi^*)$ transitions centered on the ligands. At longer wavelengths, two distinct broader and less intense MLCT bands are found at longer wavelengths corresponding to Fe–carbene $^1(d \rightarrow \pi_{\text{NHC}}^*)$ transitions (320–420 nm) and Fe–azine $^1(d \rightarrow \pi_{\text{azine}}^*)$ transitions, which extend well into the visible region (380–650 nm).⁵ Nevertheless, a clear effect of the ligand configuration can be observed (Figure 8, left and middle). On the one hand, the transitions are less intense in facial complexes due to symmetry reasons.²³ Moreover, NHC modification can result in different modulations of the $^1(d \rightarrow \pi_{\text{azine}}^*)$ bands. While more donor NHC moieties correlate well with lower-energy transitions in facial complexes, with MLCT energies varying as *fac*-C10 (bIm) > *fac*-C5 (Im) > *fac*-C9 (4-MeIm) (Figure 8, left), a no apparent trend is obtained in the meridional series (MLCT band energy: *mer*-C7 (Im) > *mer*-C11 (4-MeIm) > *mer*-C12 (bIm)) (Figure 8, middle) (*vide infra*). Indeed, bIm carbene units lead to a blue shift in facial coordination (*fac*-C10 vs *fac*-C5) but cause a red shift in meridional coordination (*mer*-C12 vs *mer*-C7).

The effect of the 6-substitution on the pyridine unit appears to be related to the relatively elongated 6-Me-pyridine–Fe interaction (Figure 8, right). Actually, *fac*-C5 (6R = Me) and *fac*-C16 (6R = Cl) show almost identical spectra in spite of

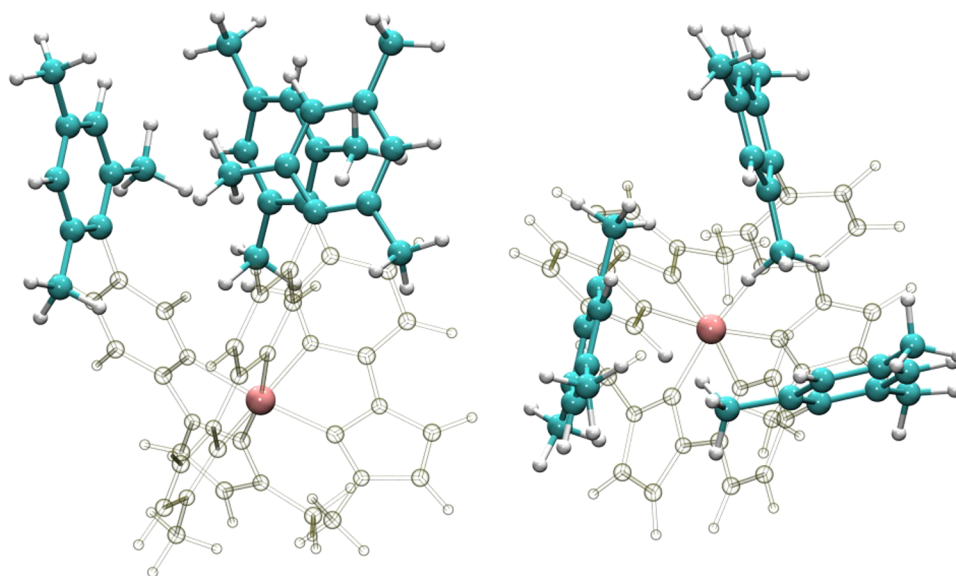


Figure 7. Side (left) and top (right) views of the *fac*-C7 structure. 5-Mes groups are highlighted as cyan (carbon) and white (hydrogen) spheres.

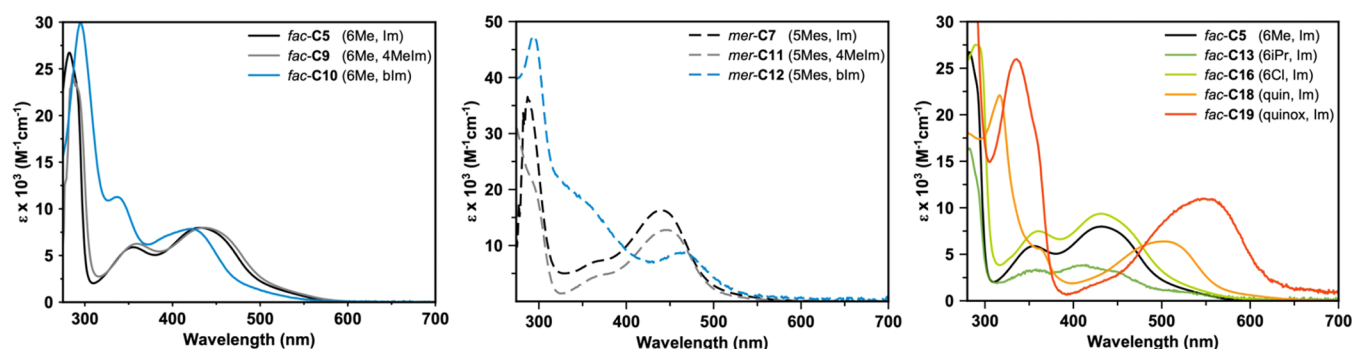


Figure 8. UV–vis spectra in air-equilibrated acetonitrile solution at room temperature to show: (left) NHC influence in facial series; (middle) NHC influence in meridional series; and (right) azine variation through substitution or π -conjugation extension.

Table 6. Photophysical and Electrochemical Data for the Facial or Meridional Fe^{II} Complexes

complex	$\lambda_{\text{abs-max}}$ (nm) [$\epsilon(\text{M}^{-1}\cdot\text{cm}^{-1})$] ^a	E_{ox} ^b [V/SCE]	E_{red} [V/SCE]	ΔE [V] ^c
<i>fac</i> -C5	285 [26 795]	0.69 (rev)	−1.59 (qr)	2.28
	355 [5891]		−1.87 (rev)	
	435 [7957]			
<i>fac</i> -C9	286 [24 398]	0.62 (rev)	−1.59 (rev)	2.21
	357 [6237]		−1.90 (qr)	
	436 [7928]			
<i>fac</i> -C10	293 [29 471]	0.95 (rev)	−1.19 (rev)	2.14
	340 [11 185]		−1.60 (rev)	
	419 [7839]			
<i>fac</i> -C13	283 [16 359]	0.81 (rev)	−1.42 (rev)	2.23
	351 [3274]		−1.91 (irr)	
	416 [3810]			
<i>fac</i> -C16	278 [25 731]	0.86 (rev)	−1.59 (irr)	2.45
	293 [27 383]			
	362 [7470]			
	428 [9332]			
<i>fac</i> -C18	317 [22 077]	0.79 (rev)	−1.41 (irr)	2.20
	367 [5157]		−1.63 (irr)	
	508 [6354]		−1.75 (irr)	
<i>fac</i> -C19	338 [25 764]	1.08 (qr)	−0.82 (irr)	1.90
	428 [1916]		−1.16 (irr)	
	555 [10 856]		−1.51 (irr)	
<i>mer</i> -C7	289 [35 856]	0.73 (rev)	−1.86 (rev)	2.59
	362 [6987]			
	444 [16 187]			
<i>mer</i> -C11	296 [19 460]	0.66 (rev)	−1.90 (rev)	2.56
	368 [4589]			
	451 [12 640]			
<i>mer</i> -C12	293 [47 267]	1.06 (rev)	−1.37 (rev)	2.43
	360 [16 852]		−1.84 (irr)	
	464 [8562]			

^aMeasured in air-equilibrated CH₃CN solution at 25 °C. ^bFirst oxidation potential. Potentials are quoted vs SCE. Recorded in CH₃CN using NBu₄PF₆ (0.1M) as supporting electrolyte at 100 mV s^{−1}; under these conditions, $E_{1/2}(\text{Fc}^+/\text{Fc}) = 0.39\text{V/SCE}$; rev = reversible; qr = quasi-reversible; irr = irreversible. ^cElectrochemical band gap ($\Delta E = E_{\text{ox}} - E_{\text{red1}}$).

their distinct electronic nature. In the case of *fac*-C13 (6R = ⁱPr), the less intense UV–vis spectrum might be attributed to the increased steric hindrance of ⁱPr in comparison with Me or Cl. In stark contrast, benzannulation of the azine unit does induce a noticeable change in the absorbance spectrum, evidencing the increased accepting character with bands red-shifted *ca.* 3200 cm^{−1} for *fac*-C18 (quinolyl) and *ca.* 5000 cm^{−1} for *fac*-C19 (quinoxalyl) with respect to *fac*-C5 (pyridyl) (Figure 8, right).

Concerning the redox properties, cyclic voltammetry of the complexes was carried out with SCE as the standard electrode and ferrocene as internal reference (Fc⁺/Fc = 0.39V/SCE in acetonitrile). At positive potentials, these bidentate *fac/mer* complexes display reversible Fe^{II} to Fe^{III} oxidations in most cases, with potentials ranging between 0.62 and 1.08 V (Table 6). These values can be nicely correlated to the π -back donation of Fe^{II} to both NHC and azine moieties, which results in higher reduction potentials due to the stabilization of the t_{2g} -like orbital (HOMO). For instance, the increasing

electron-withdrawing character on going from 4-MeIm to Im to bIm is reflected on an anodic shift of the oxidation potentials in both facial and meridional series (*fac*-C9 < *fac*-C5 < *fac*-C10 and *mer*-C11 < *mer*-C7 < *mer*-C12). The same effect is observed when the azine unit is modified, e.g., 0.69 V for *fac*-C5 (pyridyl), 0.79 V for *fac*-C18 (quinolyl), and 1.08 V for *fac*-C19 (quinoxalyl).

Noticeable differences in the cathodic events ascribed to the reduction of the ligands are obtained as well (−1.91 to −0.82 V). In comparison to C0 (−1.94 V, −1.97 V), reduction is likely to take place at the azine unit for *mer*-C7 (−1.86 V) and *mer*-C11 (−1.90 V), together with *fac*-C18 and *fac*-C19, which show drastic cathodic shifts that correspond well with their increased acceptor character and thus, lower π^* orbitals. Moreover, the introduction of more π -conjugated NHC units (bIm) seems to contribute to more delocalized LUMO, resulting in lower potentials as well (*fac*-C10 vs *fac*-C5 and *fac*-C9, *mer*-C12 vs *mer*-C7, and *mer*-C11).⁵ However, the interpretation is less straightforward for the other complexes (*fac*-C13 and *fac*-C16). In fact, the steric hindrance exerted by the azine units in facial configurations affects their coordination to the metallic center and, thus, the exact nature of the Fe–L interactions.

In consequence, these results highlight the subtle interplay between electronic effects and geometry. For facial pyridyl-based complexes, MLCT energies appear to mainly depend on the carbene donor strength (Figure 8, left and right). However, meridional complexes are more sensitive to the π -conjugation of the carbene unit, which would explain the opposite effect observed for bIm-bearing complexes *fac*-C10 (Figure 8, left) and *mer*-C12 (Figure 8, middle). In the latter case, the higher stabilization of the t_{2g} -like orbital as a result of the π -accepting character of the bIm moiety is largely offset by the concomitant stabilization of the π^* orbital, resulting in a red-shifted MLCT band. On the other hand, selection of π -extended azines as in *fac*-C18 and *fac*-C19 leads to a remarkable stabilization of the ligand π^* orbitals, nicely agreeing with the noticeable red shift of their corresponding UV–vis spectra.

CONCLUSIONS

In this contribution, we have described some ligand design guidelines to selectively access both facial and meridional isomers in azine-NHC Fe(II) complexes by means of a room-temperature protocol. As we have demonstrated, the origin of this outstanding selectivity stems from the bulkiness of the azine unit in nearby positions to the N coordinating atom. Interestingly, an increase of the steric hindrance at the α position (6-substituted derivatives) with relatively small substituents such as a methyl group or a chlorine atom resulted in a surprising *fac* configuration. In fact, considering the common orientation of these substituents, similar substitution patterns of bidentated ligands have been typically reported to lead to the *mer* isomer. Moreover, π -extended quinoline and quinoxaline moieties exerted a similar preference for facial isomerism. In the case of the highly sterically demanding mesitylene group, target complexes were only achieved upon moving away the steric hindrance to position 5 of the azine unit, where *mer* isomers were mostly obtained instead. In spite of some preliminary computational calculations, an explanation of the *fac/mer* selectivity requires a deeper investigation on the complexation mechanism, which is currently ongoing in our laboratory.

Structural characterization of these complexes has revealed that *fac* isomers possess more distorted coordination spheres than the *mer* isomers, which could be deleterious for their EE dynamics. Nevertheless, it is also reasonable to think that the presence of more interligand interactions in *fac* derivatives could impede Fe–N bond elongation, which has been shown to be the main coordinate driving the relaxation.³³ On the other hand, the nature of the NHC unit and the extension of π -conjugation appeared to be the key parameters controlling their optical and redox properties, with both isomers exhibiting distinct behaviors. The use of π -extended azines is of particular relevance due to their low-lying MLCT manifold, which results in an improved absorbance in the visible range. In addition, the possible reduction of the electronic coupling with the metal-centered states could contribute to longer-lived MLCT. However, a proper analysis of the *fac/mer* influence on the EE kinetics will be the object of a following contribution.

Thus, this work highlights the great potential of this type of complexes that capitalize on the synergetic effect of combining a certain substitution pattern at the azine unit together with NHC. As a result, nonlabile iron(II) complexes can not only be prepared with a ligand-encoded stereochemistry, but also with optoelectronic properties that can be easily fine-tuned as a function of both the azine and the NHC moieties.

ASSOCIATED CONTENT

Supporting Information

The Supporting Information is available free of charge at <https://pubs.acs.org/doi/10.1021/acsorginorgau.2c00038>.

NMR, spectroscopic and electrochemical data for complexes, and additional computational and photophysical details (PDF)

Accession Codes

CCDC 2126499–2126500 and 2126506 contain the supplementary crystallographic data for this paper. These data can be obtained free of charge via www.ccdc.cam.ac.uk/data_request/cif, or by emailing data_request@ccdc.cam.ac.uk, or by contacting The Cambridge Crystallographic Data Centre, 12 Union Road, Cambridge CB2 1EZ, UK; fax: +44 1223 336033.

AUTHOR INFORMATION

Corresponding Authors

Cristina Cebrián – Université de Lorraine, CNRS, L2CM, F-57000 Metz, France; orcid.org/0000-0002-1773-6722; Email: cristina.cebrian-avila@univ-lorraine.fr

Philippe C. Gros – Université de Lorraine, CNRS, L2CM, F-54000 Nancy, France; orcid.org/0000-0003-4905-1581; Email: philippe.gros@univ-lorraine.fr

Authors

Ulises Carrillo – Université de Lorraine, CNRS, L2CM, F-57000 Metz, France

Antonio Francés-Monerris – Departament de Química Física, Universitat de València, 46100 Burjassot, Spain; orcid.org/0000-0001-8232-4989

Anil Reddy Marri – Université de Lorraine, CNRS, L2CM, F-54000 Nancy, France; Present Address: Department of Chemistry, North Carolina State University, Raleigh, North Carolina 27695-8204, United States

Complete contact information is available at: <https://pubs.acs.org/10.1021/acsorginorgau.2c00038>

Author Contributions

The manuscript was written through contributions of all authors. All authors have given approval to the final version of the manuscript.

Funding

This research was supported by the French Agence Nationale de la Recherche (ANR-16-CE07-0013 and ANR-21-CE50-0040).

Notes

The authors declare no competing financial interest.

ACKNOWLEDGMENTS

The authors would like to acknowledge fruitful discussions with Prof. M. Desage-El Murr. A.F.-M. is grateful to the Juan de la Cierva program of the Ministerio de Ciencia e Innovación (Contract IJC2019-039297-I) for financial support. The authors are also grateful to M. Glatt and S. Rup-Jacques (LCP-A2MC) for performing the NMR experiments, S. Parant for the electrochemical experiments, and F. Dupire from the mass spectrometry MassLor platform of Lorraine University. The authors thank the PMD²X X-ray diffraction facility of the Institut Jean Barriol, Lorraine University, for X-ray diffraction measurements, data processing and analysis, and providing reports for publication: <http://crm2.univ-lorraine.fr/lab/fr/services/pmd2x>.

REFERENCES

- (1) Dabb, S. L.; Fletcher, N. C. *Mer and Fac Isomerism in Tris Chelate Diimine Metal Complexes*. *Dalton Trans.* **2015**, *44*, 4406–4422.
- (2) Yun, B.-S.; Kim, S.-Y.; Kim, J.-H.; Son, H.-J.; Kang, S. O. Homoleptic Cyclometalated Dibenzothiophene–NHC–Iridium(III) Complexes for Efficient Blue Phosphorescent Organic Light-Emitting Diodes. *J. Mater. Chem. C* **2021**, *9*, 4062–4069.
- (3) Cooke, G.; Ó Máille, G. M.; Quesada, R.; Wang, L.; Varughese, S.; Draper, S. M. Substituted Pyridazines as Ligands in Homoleptic (*Fac* and *Mer*) and Heteroleptic Ru(II) Complexes. *Dalton Trans.* **2011**, *40*, 8206–8212.
- (4) Lathion, T.; Guénee, L.; Besnard, C.; Bousseksou, A.; Piguet, C. Deciphering the Influence of Meridional versus Facial Isomers in Spin Crossover Complexes. *Chem. - Eur. J.* **2018**, *24*, 16873–16888.
- (5) Magra, K.; Francés-Monerris, A.; Cebrián, C.; Monari, A.; Haacke, S.; Gros, P. C. Bidentate Pyridyl-NHC Ligands: Synthesis, Ground and Excited State Properties of Their Iron(II) Complexes and the Role of the *Fac/Mer* Isomerism. *Eur. J. Inorg. Chem.* **2022**, No. e202100818.
- (6) Lee, J.; Chen, H.-F.; Batagoda, T.; Coburn, C.; Djurovich, P. I.; Thompson, M. E.; Forrest, S. R. Deep Blue Phosphorescent Organic Light-Emitting Diodes with Very High Brightness and Efficiency. *Nat. Mater.* **2016**, *15*, 92–98.
- (7) Ehnbo, A.; Ghosh, S. K.; Lewis, K. G.; Gladysz, J. A. Octahedral Werner Complexes with Substituted Ethylenediamine Ligands: A Stereochemical Primer for a Historic Series of Compounds Now Emerging as a Modern Family of Catalysts. *Chem. Soc. Rev.* **2016**, *45*, 6799–6811.
- (8) Shopov, D. Y.; Rudshiteyn, B.; Campos, J.; Batista, V. S.; Crabtree, R. H.; Brudvig, G. W. Stable Iridium(IV) Complexes of an Oxidation-Resistant Pyridine-Alkoxide Ligand: Highly Divergent Redox Properties Depending on the Isomeric Form Adopted. *J. Am. Chem. Soc.* **2015**, *137*, 7243–7250.
- (9) Metherell, A. J.; Cullen, W.; Stephenson, A.; Hunter, C. A.; Ward, M. D. *Fac* and *Mer* Isomers of Ru(II) Tris(Pyrazolyl-Pyridine) Complexes as Models for the Vertices of Coordination Cages: Structural Characterisation and Hydrogen-Bonding Characteristics. *Dalton Trans.* **2014**, *43*, 71–84.
- (10) Morozumi, T.; Matsuoka, R.; Nakamura, T.; Nabeshima, T. Solvent-Dependent *Fac/Mer* -Isomerization and Self-Assembly of Triply Helical Complexes Bearing a Pivot Part. *Chem. Sci.* **2021**, *12*, 7720–7726.
- (11) Kieffer, M.; Pilgrim, B. S.; Ronson, T. K.; Roberts, D. A.; Aleksanyan, M.; Nitschke, J. R. Perfluorinated Ligands Induce Meridional Metal Stereochemistry to Generate M₃L₁₂, M₁₀L₁₅, and M₁₂L₁₈ Prisms. *J. Am. Chem. Soc.* **2016**, *138*, 6813–6821.
- (12) Coe, B. J.; Glenwright, S. J. Trans-Effects in Octahedral Transition Metal Complexes. *Coord. Chem. Rev.* **2000**, *203*, 5–80.
- (13) Deorukhkar, N.; Besnard, C.; Guénee, L.; Piguet, C. Tuning Spin-Crossover Transition Temperatures in Non-Symmetrical Homoleptic Meridional/Facial [Fe(Didentate)₃]²⁺ Complexes: What for and Who Cares about It? *Dalton Trans.* **2021**, *50*, 1206–1223.
- (14) Howson, S. E.; Allan, L. E. N.; Chmel, N. P.; Clarkson, G. J.; Deeth, R. J.; Faulkner, A. D.; Simpson, D. H.; Scott, P. Origins of Stereoselectivity in Optically Pure Phenylethanaminopyridine Tris-Chelates M(NN')₃ⁿ⁺ (M = Mn, Fe, Co, Ni and Zn). *Dalton Trans.* **2011**, *40*, 10416–10433.
- (15) Tidmarsh, I. S.; Faust, T. B.; Adams, H.; Harding, L. P.; Russo, L.; Clegg, W.; Ward, M. D. Octanuclear Cubic Coordination Cages. *J. Am. Chem. Soc.* **2008**, *130*, 15167–15175.
- (16) Fletcher, N. C.; Brown, R. T.; Doherty, A. P. New Stepwise Approach to Inert Heterometallic Triple-Stranded Helicates. *Inorg. Chem.* **2006**, *45*, 6132–6134.
- (17) Fletcher, N. C.; Martin, C.; Abraham, H. J. Enantiomeric Programming in Tripodal Transition Metal Scaffolds. *New J. Chem.* **2007**, *31*, 1407.
- (18) Brisig, B.; Constable, E. C.; Housecroft, C. E. Metal-Directed Assembly of Combinatorial Libraries—Principles and Establishment of Equilibrated Libraries with Oligopyridine Ligands. *New J. Chem.* **2007**, *31*, 1437.
- (19) Morita, H.; Akine, S.; Nakamura, T.; Nabeshima, T. Exclusive Formation of a Meridional Complex of a Tripodand and Perfect Suppression of Guest Recognition. *Chem. Commun.* **2021**, *57*, 2124–2127.
- (20) Kobayashi, Y.; Hoshino, M.; Kameda, T.; Kobayashi, K.; Akaji, K.; Inuki, S.; Ohno, H.; Oishi, S. Use of a Compact Tripodal Tris(Bipyridine) Ligand to Stabilize a Single-Metal-Centered Chirality: Stereoselective Coordination of Iron(II) and Ruthenium(II) on a Semirigid Hexapeptide Macrocyclic. *Inorg. Chem.* **2018**, *57*, 5475–5485.
- (21) Moriuchi, T.; Mao, L.; Wu, H.-L.; Ohmura, S. D.; Watanabe, M.; Hirao, T. Synthesis of Facial Cyclometalated Iridium(III) Complexes Triggered by Tripodal Ligands. *Dalton Trans.* **2012**, *41*, 9519–9525.
- (22) Huang, S.-Y.; Qian, M.; Pierre, V. C. The Ligand Cap Affects the Coordination Number but Not Necessarily the Affinity for Anions of Tris-Bidentate Europium Complexes. *Inorg. Chem.* **2020**, *59*, 4096–4108.
- (23) Magra, K.; Domenichini, E.; Francés-Monerris, A.; Cebrián, C.; Beley, M.; Darari, M.; Pastore, M.; Monari, A.; Assfeld, X.; Haacke, S.; Gros, P. C. Impact of the *Fac/Mer* Isomerism on the Excited-State Dynamics of Pyridyl-Carbene Fe(II) Complexes. *Inorg. Chem.* **2019**, *58*, 5069–5081.
- (24) Tamayo, A. B.; Alleyne, B. D.; Djurovich, P. I.; Lamansky, S.; Tsyba, I.; Ho, N. N.; Bau, R.; Thompson, M. E. Synthesis and Characterization of Facial and Meridional Tris-Cyclometalated Iridium(III) Complexes. *J. Am. Chem. Soc.* **2003**, *125*, 7377–7387.
- (25) McDonald, A. R.; Lutz, M.; von Chranowski, L. S.; van Klink, G. P. M.; Spek, A. L.; van Koten, G. Probing the *Mer* - to *Fac* -Isomerization of Tris-Cyclometalated Homo- and Heteroleptic (C,N)₃ Iridium(III) Complexes. *Inorg. Chem.* **2008**, *47*, 6681–6691.
- (26) McGee, K. A.; Mann, K. R. Selective Low-Temperature Syntheses of Facial and Meridional Tris-Cyclometalated Iridium(III) Complexes. *Inorg. Chem.* **2007**, *46*, 7800–7809.
- (27) Jarenmark, M.; Fredin, L. A.; Hedberg, J. H. J.; Doverbratt, I.; Persson, P.; Abrahamsson, M. A Homoleptic Trisbidentate Ru(II) Complex of a Novel Bidentate Biheteroaromatic Ligand Based on

Quinoline and Pyrazole Groups: Structural, Electrochemical, Photo-physical, and Computational Characterization. *Inorg. Chem.* **2014**, *53*, 12778–12790.

(28) Leis, W.; Argüello Cordero, M. A.; Lochbrunner, S.; Schubert, H.; Berkefeld, A. A Photoreactive Iron(II) Complex Luminophore. *J. Am. Chem. Soc.* **2022**, *144*, 1169–1173.

(29) Chábera, P.; Kjaer, K. S.; Prakash, O.; Honarfar, A.; Liu, Y.; Fredin, L. A.; Harlang, T. C. B.; Lidin, S.; Uhlig, J.; Sundström, V.; Lomoth, R.; Persson, P.; Wärnmark, K. Fe^{II} Hexa N-Heterocyclic Carbene Complex with a 528 Ps Metal-to-Ligand Charge-Transfer Excited-State Lifetime. *J. Phys. Chem. Lett.* **2018**, *9*, 459–463.

(30) Kjær, K. S.; Kaul, N.; Prakash, O.; Chábera, P.; Rosemann, N. W.; Honarfar, A.; Gordivska, O.; Fredin, L. A.; Bergquist, K.-E.; Häggström, L.; Ericsson, T.; Lindh, L.; Yartsev, A.; Styring, S.; Huang, P.; Uhlig, J.; Bendix, J.; Strand, D.; Sundström, V.; Persson, P.; Lomoth, R.; Wärnmark, K. Luminescence and Reactivity of a Charge-Transfer Excited Iron Complex with Nanosecond Lifetime. *Science* **2019**, *363*, 249–253.

(31) Steube, J.; Pápcke, A.; Bokareva, O.; Reuter, T.; Demeshko, S.; Schoch, R.; Hohloch, S.; Meyer, F.; Kühn, O.; Lochbrunner, S.; Heinze, K.; Bauer, M. S. Janus-type dual emission of a Cyclometalated Iron(III) Complex. *Research Square* **2020**, DOI: 10.21203/rs.3.rs-64316/v1

(32) Braun, J. D.; Lozada, I. B.; Kolodziej, C.; Burda, C.; Newman, K. M. E.; van Lierop, J.; Davis, R. L.; Herbert, D. E. Iron(II) Coordination Complexes with Panchromatic Absorption and Nanosecond Charge-Transfer Excited State Lifetimes. *Nat. Chem.* **2019**, *11*, 1144–1150.

(33) Francés-Monerris, A.; Magra, K.; Darari, M.; Cebrián, C.; Beley, M.; Domenichini, E.; Haacke, S.; Pastore, M.; Assfeld, X.; Gros, P. C.; Monari, A. Synthesis and Computational Study of a Pyridylcarbene Fe(II) Complex: Unexpected Effects of *Fac/Mer* Isomerism in Metal-to-Ligand Triplet Potential Energy Surfaces. *Inorg. Chem.* **2018**, *57*, 10431–10441.

(34) Francés-Monerris, A.; Gros, P. C.; Assfeld, X.; Monari, A.; Pastore, M. Toward Luminescent Iron Complexes: Unravelling the Photophysics by Computing Potential Energy Surfaces. *ChemPhotoChem* **2019**, *3*, 666–683.

(35) Magra, K.; Darari, M.; Domenichini, E.; Francés-Monerris, A.; Cebrián, C.; Beley, M.; Pastore, M.; Monari, A.; Assfeld, X.; Haacke, S.; Gros, P. C. Photophysical Investigation of Iron(II) Complexes Bearing Bidentate Annulated Isomeric Pyridine-NHC Ligands. *J. Phys. Chem. C* **2020**, *124*, 18379–18389.

(36) Hong, Y.; Jarrige, L.; Harms, K.; Meggers, E. Chiral-at-Iron Catalyst: Expanding the Chemical Space for Asymmetric Earth-Abundant Metal Catalysis. *J. Am. Chem. Soc.* **2019**, *141*, 4569–4572.

(37) Onggo, D.; Hook, J. M.; Rae, A. D.; Goodwin, H. A. The Influence of Steric Effects in Substituted 2,2'-Bipyridine on the Spin State of Iron(II) in [FeN₆]⁺² Systems. *Inorg. Chim. Acta* **1990**, *173*, 19–30.

(38) Zang, Y.; Kim, J.; Dong, Y.; Wilkinson, E. C.; Appelman, E. H.; Que, L. Models for Nonheme Iron Intermediates: Structural Basis for Tuning the Spin States of Fe(TPA) Complexes. *J. Am. Chem. Soc.* **1997**, *119*, 4197–4205.

(39) Seredyuk, M.; Gaspar, A. B.; Kusz, J.; Bednarek, G.; Gütllich, P. Variable-Temperature X-Ray Crystal Structure Determinations of {Fe[Tren(6-Mepy)₃]}(ClO₄)₂ and {Zn[Tren(6-Mepy)₃]}(ClO₄)₂ Compounds: Correlation of the Structural Data with Magnetic and Mössbauer Spectroscopy Data. *J. Appl. Crystallogr.* **2007**, *40*, 1135–1145.

(40) Jahro, I. S.; Onggo, D.; Ismunandar; Rahayu, S. I.; Muñoz, M. C.; Gaspar, A. B.; Seredyuk, M.; Gütllich, P.; Real, J. A. Synthesis, Crystal Structure and Magnetic Properties of the Spin Crossover System [Fe(pq)₃]²⁺. *Inorg. Chim. Acta* **2008**, *361*, 4047–4054.

(41) Ketkaew, R.; Tantirungrotechai, Y.; Harding, P.; Chastanet, G.; Guionneau, P.; Marchivie, M.; Harding, D. J. OctaDist: A Tool for Calculating Distortion Parameters in Spin Crossover and Coordination Complexes. *Dalton Trans.* **2021**, *50*, 1086–1096.

(42) Abernethy, C. D.; Codd, G. M.; Spicer, M. D.; Taylor, M. K. A Highly Stable N-Heterocyclic Carbene Complex of Trichloro-Oxo-Vanadium(V) Displaying Novel Cl–C_{carbene} Bonding Interactions. *J. Am. Chem. Soc.* **2003**, *125*, 1128–1129.

(43) Frisch, M. J.; Trucks, G. W.; Schlegel, H. B.; Scuseria, G. E.; Robb, M. a.; Cheeseman, J. R.; Scalmani, G.; Barone, V.; Petersson, G. a.; Nakatsuji, H.; Li, X.; Caricato, M.; Marenich, V.; Bloino, J.; Janesko, B. G.; Gomperts, R.; Mennucci, B.; Hratchian, H. P.; Ortiz, J. V.; Izmaylov, F.; Sonnenberg, J. L.; Williams, Ding, F.; Lipparini, F.; Egidi, F.; Goings, J.; Peng, B.; Petrone, A.; Henderson, T.; Ranasinghe, D.; Zakrzewski, V. G.; Gao, J.; Rega, N.; Zheng, G.; Liang, W.; Hada, M.; Ehara, M.; Toyota, K.; Fukuda, R.; Hasegawa, J.; Ishida, M.; Nakajima, T.; Honda, Y.; Kitao, O.; Nakai, H.; Vreven, T.; Throssell, K.; Montgomery, J., Jr.; Peralta, J. E.; Ogliaro, F.; Bearpark, M. J.; Heyd, J. J.; Brothers, E. N.; Kudin, K. N.; Staroverov, V. N.; Keith, T.; Kobayashi, R.; Normand, J.; Raghavachari, K.; Rendell, P.; Burant, J. C.; Iyengar, S. S.; Tomasi, J.; Cossi, M.; Millam, J. M.; Klene, M.; Adamo, C.; Cammi, R.; Ochterski, J. W.; Martin, R. L.; Morokuma, K.; Farkas, O.; Foresman, J. B.; Fox, D. J. *Gaussian 16*, Revision C.01; Gaussian, Inc.: Wallingford CT, 2016.

(44) Grimme, S.; Antony, J.; Ehrlich, S.; Krieg, H. A Consistent and Accurate Ab Initio Parametrization of Density Functional Dispersion Correction (DFT-D) for the 94 Elements H-Pu. *J. Chem. Phys.* **2010**, *132*, No. 154104.

(45) Mennucci, B. Polarizable Continuum Model. *WIREs Comput. Mol. Sci.* **2012**, *2*, 386–404.

(46) Isayev, O.; Gorb, L.; Leszczynski, J. Theoretical Calculations: Can Gibbs Free Energy for Intermolecular Complexes Be Predicted Efficiently and Accurately? *J. Comput. Chem.* **2007**, *28*, 1598–1609.

(47) Riplinger, C.; Neese, F. An Efficient and near Linear Scaling Pair Natural Orbital Based Local Coupled Cluster Method. *J. Chem. Phys.* **2013**, *138*, No. 34106.

(48) Neese, F.; Wennmohs, F.; Becker, U.; Riplinger, C. The ORCA Quantum Chemistry Program Package. *J. Chem. Phys.* **2020**, *152*, No. 224108.

(49) Liakos, D. G.; Guo, Y.; Neese, F. Comprehensive Benchmark Results for the Domain Based Local Pair Natural Orbital Coupled Cluster Method (DLPNO-CCSD(T)) for Closed- and Open-Shell Systems. *J. Phys. Chem. A* **2020**, *124*, 90–100.

(50) Loveday, O.; Echeverría, J. Methyl Groups as Widespread Lewis Bases in Noncovalent Interactions. *Nat. Commun.* **2021**, *12*, No. 5030.